AerospaceEurope Conference2021
WARSAW, POLAND | 23 -26 NOVEMBER 2021
CEAS Council of European Aerospace Societies

STAGE SEPARATION DYNAMICS OPTIMIZATION VIA AERODYNAMICS AND FLIGHT DYNAMICS SIMULATION TO AVOID COLLISION DURING TSTO SEPARATION BY AERODYNAMICS AND FLIGHT DYNAMICS SIMULATION

Shinnosuke Yoshida[1], Masahiro Kanazaki[1] & Yusuke Yamada[1]

[1]Department of Aeronautics and Astronautics, Graduate School of System Design, Tokyo Metropolitan University 1

Abstract

Herein, we discuss the optimization of the stage separation sequence based on aerodynamics, flight dynamics, and evolutionary algorithms (EAs) for winged two-stage-to-orbit (TSTO). In the TSTO model considered in this study, the same vehicle geometry, consisting of a main wing, V-tail wings, and fuselage, was employed as a booster and orbiter. An unstructured mesh-based computational fluid dynamics (CFD) model was employed to collect aerodynamic data. The engine plume was simulated using the CFD. The stage separation dynamics were optimized using EA with simultaneous minimization of the total control moment and time, except for the shock wave interaction area. The CFD results reveal that the TSTO could not gain enough aerodynamic force to separate the booster and orbiter when they were close to each other. Therefore, this TSTO concept requires an appropriate control force to avoid collisions. The optimization enabled the TSTO to be successfully separated through a suitable design of the control moment.

Keywords: CFD, Optimization, Aerodynamic Characteristics, Stage Separation

1. Introduction

Next-generation space transportation systems are required to be safe, easily operable, and cost-effective. A winged two-stage-to-orbit (TSTO) space vehicle is a promising concept for satisfying these requirements, and various studies [2][4] have been conducted in this regard. A team including the authors of this paper has been conducting research and development on the TSTO [2][4] based on a highly manageable experimental space (HIMES) flight vehicle, which has been studied at the Institute of Space and Astronautical Science (ISAS). The TSTO concept assumes that the HIMES aircraft is similar to an orbiter and booster and that these components are connected to each other. The booster accelerates the orbiter to hypersonic speed and is then detached from the orbiter and lands on the runway. The orbiter reenters the atmosphere, glides into the orbit, and lands on the runway. This launch sequence is shown in Fig. 1. The TSTO concept assumes separation at hypersonic speed. In such a case, aerodynamic interference effects between the two vehicles are observed owing to the complex flow field caused by shock wave interference and plume flow. Iwafuji et al. performed computational fluid dynamics (CFD) calculations considering both the TSTO two-body problem and the plume flow at hypersonic speeds and discussed the complex interference between the shock waves and the plume exhaust flow generated by the orbiter and the booster[4]. Furthermore, the aerodynamic forces generated by the two airframes suggest that uncontrolled separation may result in collisions between airframes.
Coupled calculations involving fluid dynamics and flight dynamics [2] and separation motion simulations using the polymerized grid method [4] were used to evaluate the separation motion to avoid collisions. As per the present TSTO concept, it is necessary to evaluate the feasibility of separation by considering the complex flow field to determine the degree of control required for proper separation.

The purpose of this study is to evaluate the separation motion in the TSTO concept by optimizing the separation motion considering the aerodynamic interference effect between lifting bodies. To this end, assuming the TSTO separation, CFD simulation is first performed under hypersonic speeds, while the relative positions of the booster and orbiter are varied, and an aerodynamic database is constructed according to the proximity of the aircraft. Next, we investigate the characteristics of the separation motion of the TSTO concept by performing aerodynamic flight-coupled calculations based on the database and optimization of the separation motion using an evolutionary algorithm (EA).

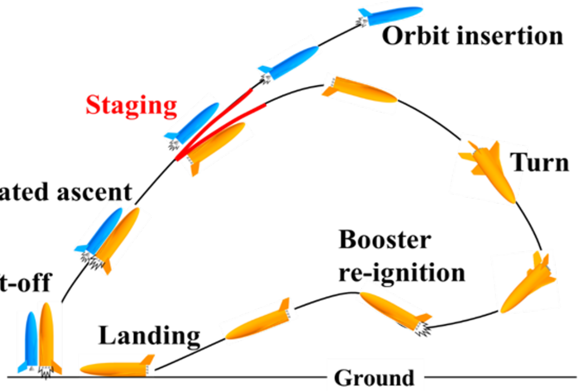

Figure 1 – TSTO concept.

2. Design Problem for Stage Separation of TSTO

2.1 Design Target

This paper focuses on the TSTO concept [1], which represents a vehicle capable of transporting a 10.0 [t] payload to a low orbit at an altitude of 35,000 [m]. The TSTO concept is designed based on the HIMES flying vehicle, which has been studied at ISAS. This vehicle comprises a booster and orbiter, which have similar configurations, and the lower surface of the fuselage is connected to both components to function as a TSTO. In this study, we focused on the motion calculation for 3 s from the start of the separation sequence. During the separation sequence, the engine is assumed to run only on the orbiter, and separation is performed by applying a provisional control moment around the center of gravity of the orbiter. Table 1 shows the characteristics of each component at the start of separation.

Table 1 – Dimensions of the TSTO

Booster	Fuselage length	40.8 [m]
	Fuselage diameter	8.9 [m]
	Fuel mass	23.9 [t]
	Empty mass	55.7 [t]
	Moment of Inertia	2.46×10^{7} [kg/m^2]
	Center of gravity (from the nose)	22.2 [m]
Orbiter	Fuselage length	34.7 [m]
	Fuselage diameter	7.6 [m]
	Fuel mass	158.7 [t]
	Empty mass	33.1 [t]
	Moment of Inertia	8.46×10^{6} [kg/m^2]
	Center of gravity (from the nose)	15.2 [m]
	Thrust	1960.0 [kN]
	Specific impulse	340.0[s]

2.2 Formulation

Considering the effects of shock wave interference on the aircraft and flight, it is better to separate the booster and orbiter quickly while minimizing the control moment applied to avoid collisions between the orbiter and booster. Therefore, we set two objective functions for the optimization of the separation motion: minimization of the M_{total} of the control moment coefficients $C_{\text{m}_\text{c}\text{ontrol}}$ for the orbiter, and minimization of the time t_e until the orbiter is beyond the interference range of the shock wave generated by the booster.

$$\text{Minimize} \quad t_\text{e} \tag{1}$$
$$\text{Maximize} \quad M_{\text{total}} \tag{2}$$
$$\text{subject to} \quad \Delta z/D \leq 0.0,\ \Delta\theta \leq 0.0. \tag{3}$$

In this study, the separation motion is promoted by providing a tentative control moment to the orbiter's center of gravity as a design variable. The control moment coefficient $C_{\text{m}_\text{c}\text{ontrol}}$ is expressed as a time series. The maximum value of $\Delta C_{\text{m}_\text{c}\text{ontrol}}$ is 0.3 [-], the minimum value is -0.3 [-], and the extent to which $\Delta C_{\text{m}_\text{c}\text{ontrol}}$ can change in 1 s is 0.6 [-]. A total of 15 inputs are provided in 1 s, and $\Delta C_{\text{m}_\text{c}\text{ontrol}}$ is a design variable.

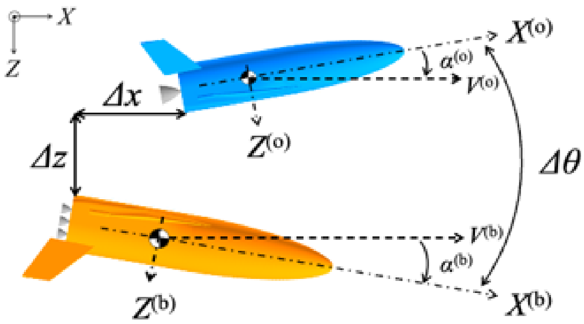

Figure 2 – Coordinate system for TSTO.

2.2.1 Definition of Shock Wave Interference Range

The shock wave interference range included in the objective function of the optimization is defined in this study. Figure 3 shows the CFD results for the single-machine form of the booster and depicts the isosurface of the normal Mach number = 1 [8]. The red area in Fig. 3 denotes the shock wave range, and it is determined whether the orbiter is within this range.

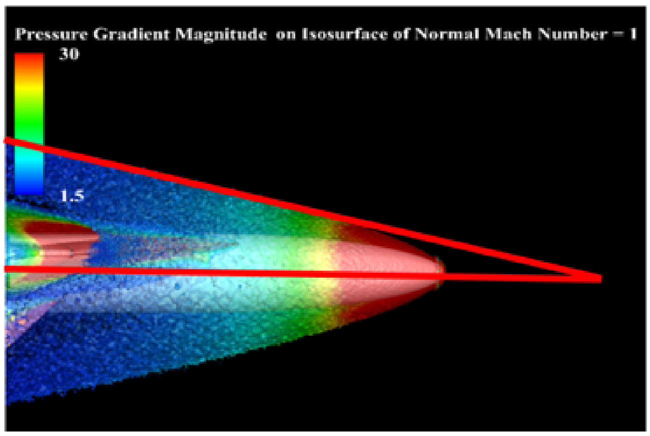

Figure 3 – Definition of shock interaction region.

2.3 Computational Condition

Using CFD, we computed the flow field at Mach number $M = 6.8$ and Reynolds number $Re = 2.0 \times 10^6$, assuming flight at an altitude of 40,500 km. To simulate the plume exhaust flow, the static pressure, temperature, and velocity were set as boundary conditions at the exit of the orbiter nozzle. The specific heat ratio is assumed to be $\gamma = 1.4$, and the pressure, temperature, and density of the exhaust flow were adjusted to match those under actual conditions [4]. The boundary conditions at the nozzle outlet are also provided. The static pressure is $Pa = 3552.2[Pa]$, the static temperature is $T = 1172.61[K]$, and the air density is $3078.46[kg/m^3]$

3. Stage Separation Optimization via Evolutionary Algorithms

3.1 Constrained Evolutionary Algorithms

In this study, we use an EA to solve the optimization problem. EA is a learning algorithm that mimics the evolutionary processes of organisms that adapt to their environment. It searches for solutions by repeatedly performing evolutionary operations, such as selection, crossover, and mutation, on each individual in a population.

In this study, we optimized the separation motion using the constrained non-dominated sorting genetic algorithm-II (CNSGA-II) [1], which is an evolutionary computation method based on the concept of domination considering the total number of constraint violations. In CNSGA-II, which involves constraint handling incorporated into NSGA-II, when a solution that does not satisfy the constraint (infeasible solution) is obtained, the amount of constraint violation is reduced to a minimum. The solution selection procedure for CNSGA-II was performed in the following order: In CNSGA-II, the solution selection procedure was performed in the following order:

1. In the case of only feasible solutions, the objective function is evaluated, and the solution is selected.
2. When both feasible and infeasible solutions are obtained, the feasible solution is selected.
3. When only infeasible solutions are present, the constraint-violating quantity is evaluated instead of the objective function, and the solution is selected.

3.2 Aerodynamic-Flight Simulation

The equations of motion for the booster and orbiter were solved independently. Subsequently, the aerodynamic coefficients are updated from the relative positions, angles, and angles of attack of the two components and are used in the next step of the motion calculation. The equations of motion are solved numerically using the fourth-order accurate Runge-Kutta method. The aerodynamic coefficients were obtained from the aerodynamic database provided in Section 3.4 However, if the input lies beyond the range of the aerodynamic database, the aerodynamic coefficients determined via the CFD calculations for the isolated forms of the booster and orbiter were used.

In this study, separation was performed in two phases, as shown in Figure 5.

3.3 Aerodynamic Database

The relative positions of the booster and orbiter are defined as follows to construct the aerodynamic database:

$$\begin{aligned}
&\Delta z/D = 1/20, 1/2, 1.0 \\
&\Delta x/L = 0.0, 1/20, 1/10, 1/3, 1/2 \\
&\Delta\theta = 0.0, 5.0, 10.0[^\circ] \\
&\alpha = 0.0, -3.0, -5.0[^\circ]
\end{aligned} \tag{4}$$

where x and z are the horizontal and vertical coordinates, respectively, θ is the angle formed by the anises of the orbiter and the booster, and α is the angle of attack. The aerodynamic coefficients acting on the aircraft are treated as functions of the angle of attack and relative position of the aircraft, and they are called from the equations of motion. The Kriging method [5][7][6] is used to estimate the aerodynamics. The sample calculations for constructing the aerodynamic model using the Kriging method were based on the CFD results shown in Section 3.4

3.4 Computation Fluid Dynamics

In this study, we used the three-dimensional compressible Navier–Stokes equations as the governing equations and solved the Reynolds-averaged Navier–Stokes (RANS) equations to obtain the time-averaged field by solving the Reynolds-averaged governing equations. The spatial discretization method was the cell-node method of the finite volume method. The turbulence model was the two-equation model, shear stress transport (SST)-2003sust [9]. The nonviscous flux calculation used Harten-Lax-Van-Leer-Eingeld [10], and the gradient calculation method used the G-G-based weighted least square method . The Lower-Upper Symmetric Gauss-Seidel (LU-SGS) implicit method [11] was used for the time integration method. FAST Aerodynamic Routuins (FaSTAR), developed by JAXA, were used as the computational solver.

An unstructured grid was adopted for the computational grid, and tetra, prism, and hexagonal elements were used for spatial grid formation. To resolve the boundary layer of the high-Reynolds number flow, prismatic layers were placed near the surface, and the minimum grid width of the first layer was set such that $y+$ was less than 1. The number of lattice points is approximately 20 million, and the minimum lattice width is 5.09×10^{-6} [-] in the dimensionless height of the boundary layer. A mixed-element grid generator in three dimensions (MEGG3D) [3], an unstructured grid generation software program developed by JAXA, was used as the grid generation tool.

4. Results and Discussions

4.1 Aerodynamic Characteristics of the Target TSTO

Figure 4 shows C_{m} for the case where $\Delta x/L$=0.0, $\Delta\theta$=0.0 and $\Delta z/D$ is changed. Figure 4 shows that when $\Delta z/D$ is small, the pitching moment of the booster and the orbiter is generated in the direction of the approaching nose section, a collision at the nose is possible. In contrast, when $\Delta z/D$ is large, the pitching moment is generated in the direction of the nose separation, which increases the distance between the aircraft and the aerodynamic forces that facilitate separation. In addition, C_{m} is similar to the CFD results for a single-plane configuration when $\Delta z/D$=1.0, which indicates that the aerodynamic interference effect can be neglected when the distance between the aircraft is large.

4.2 Separation Motion Optimization Results

In this section, the results of solving the multi-objective optimization problem shown in Eq. 3 are discussed. Figure 5 shows the distribution of feasible solutions via optimization for the case in which the constrained force of the separation mechanism is not considered. Fig. 5 shows a trade-off between the time t_{e} until the orbiter leaves the shock wave interference range of booster and the total control moment M_{total} applied to the orbiter. However, the difference between the largest and smallest t_{e} in the non-dominated solution set is only approximately 0.3 [s]; this indicates that there is no significant improvement in t_{e} owing to the difference in control moments.

The flight histories of the t_{e} minimum solution and the M_{total} minimum solution are shown in Fig. 6. Figure 6(a) shows that the t_{e} minimum solution increases $\Delta z/D$ compared with the M_{total} minimum solution. This is because, as shown in Fig. 6(b) and (c), the t_{e} minimum solution yields a larger control moment and increases the difference between the pitch angles of the orbiter and the booster; this increases the inclination of the orbiter relative to the direction of the booster's nose, and the orbiter thrust acts to increase $\Delta z/D$. In the M_{total} minimum solution, the pitch angles of the booster and orbiter are similar, and hence, the increase in $\Delta z/D$ remains small. Thus, the two planes are moving almost parallel and are within the shock wave interference range for a long time.

In both solutions, both the booster and orbiter separate with increasing pitch angle. This is because, as described in Section 4.1, the booster is subjected to a pitching moment in the head-down direction when the aircraft is in close proximity, whereas the orbiter is subjected to a control moment in the pitch-up direction to avoid a collision. Therefore, both aircraft move with an increasing pitch angle. However, this is not a realistic separation motion because of the stall that occurs at a high angle of attack.

4.3 Aerodynamic Characteristics During Separation Motions

In this section, we present visualizations of the flow field during the motion in 1.0 [s] increments from t = 0.0 [s] to 3.0 [s] for the t_{e} minimum solution. Figure 7 shows the shock waves generated by the

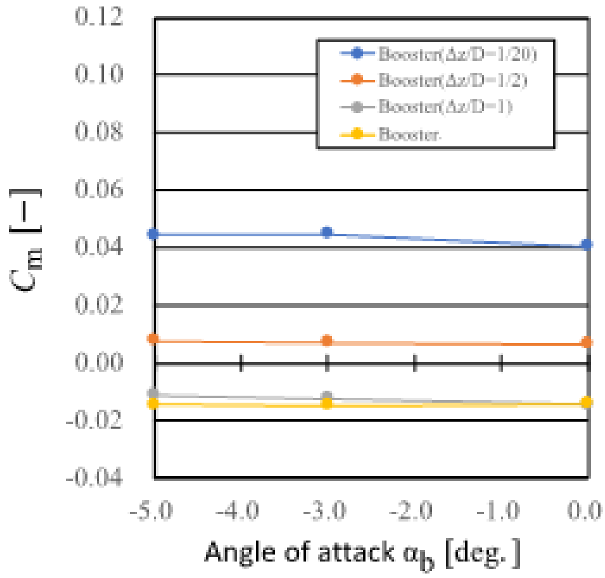

(a)

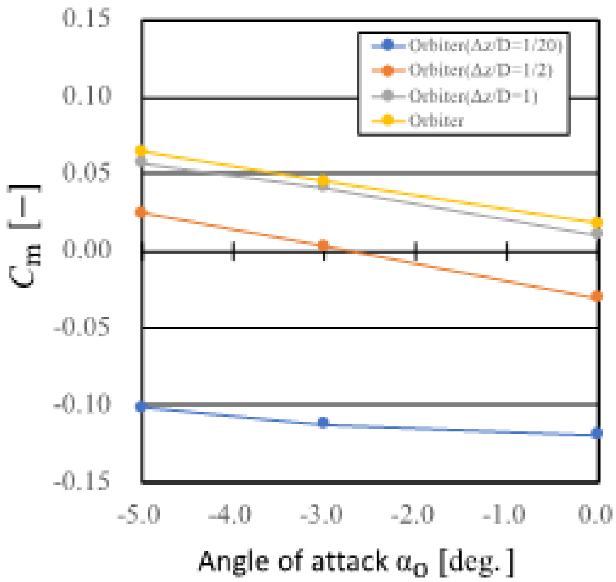

(b)

Figure 4 – Aerodynamic coefficient.(a)C_m for the booster, and(b)C_m for the orbiter.

booster and orbiter during the separation motion. From t = 0.0 to 2.0 [s], three or four pressure peaks appear at t = 0.0 [s]. At t = 1.0 [s], a pressure peak was observed only in the rear part of the aircraft. Although no interference is provided by the shock waves generated from the nose, the shock waves generated from the rear part seem to interfere.

5. Conclusions

In this study, the aerodynamic characteristics and characteristics of the separation motion of the TSTO concept were investigated. Specifically, a separation motion optimization framework considering aerodynamic interference effects was constructed using a multiobjective evolutionary computation method, global solution sets were obtained, and possible collision avoidance during separation was discussed. A high-order accurate viscosity calculation was applied for the calculation of the motion. In the multiobjective optimization, the objective functions are the minimization of the sum of the control moments given to Orbiter and the minimization of the time until Orbiter leaves the shock wave range of the booster. The optimization results showed that the orbiter can be separated without collision by applying appropriate control to the orbiter, and that there is a trade-off between the

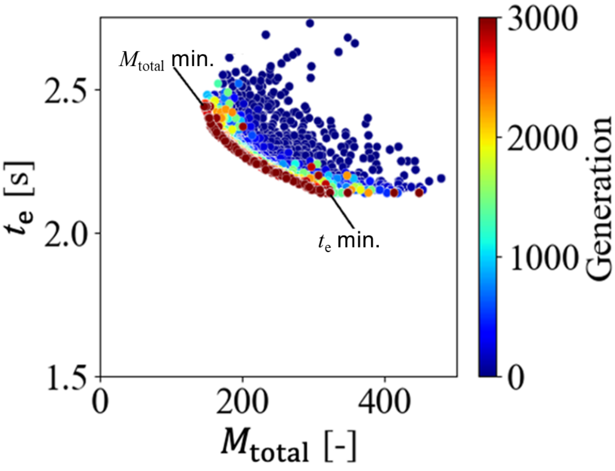

Figure 5 – Solutions space obtained by MOEA.

total control moment applied to the orbiter and the time required for the orbiter to leave the shock wave range of the booster. Then, the aerodynamic characteristics during the separation motion were discussed, in which the time until the Orbiter leaves the interference range of the Booster's shock wave was minimized. Therefore, it was understood that the plume flow of the orbiter interferes with the booster, although the orbiter is subjected to less shock wave interference from the booster when the two aircraft separate quickly. However, it is understood that the plume flow of Orbiter interferes with the booster. Because the interference of plume flow may cause damage to the airframe, it is necessary to take measures against the interference of Orbiter's plume flow with the boost in the future. In this study, a moment was applied to the center of gravity of the orbiter as a control for separation, but more advanced separation motion simulations will be possible by considering more detailed controllers and separation mechanisms.

6. Copyright Statement

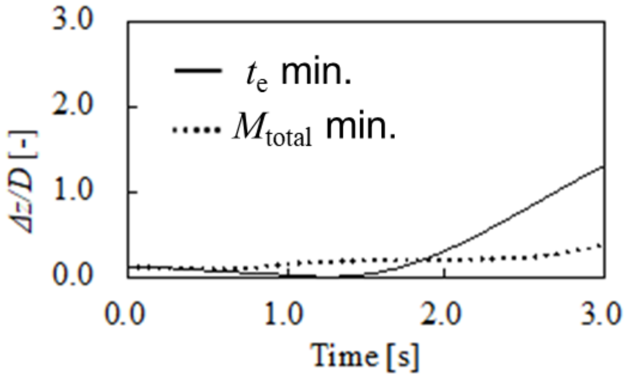

(a)

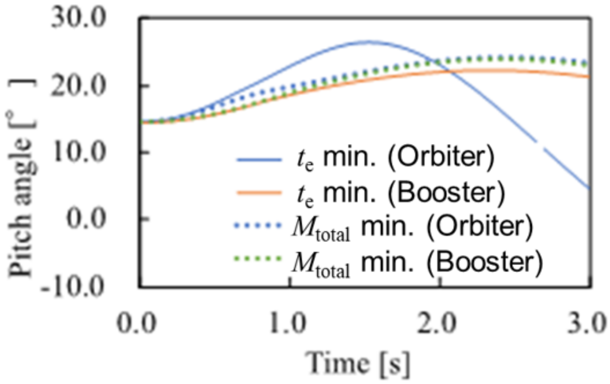

(b)

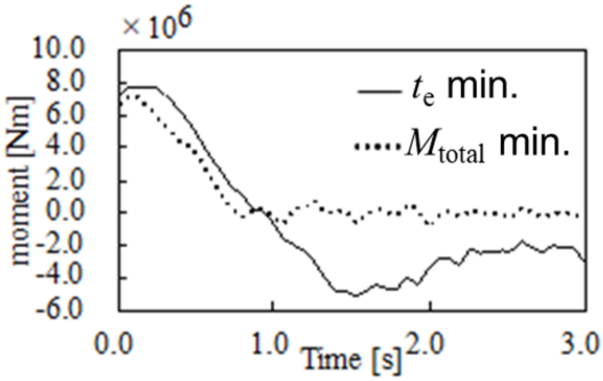

(c)

Figure 6 – Trajectories of obtained solutions.(a)$t-\Delta z/D$, (b) -pitch angle, and (c) -moment.

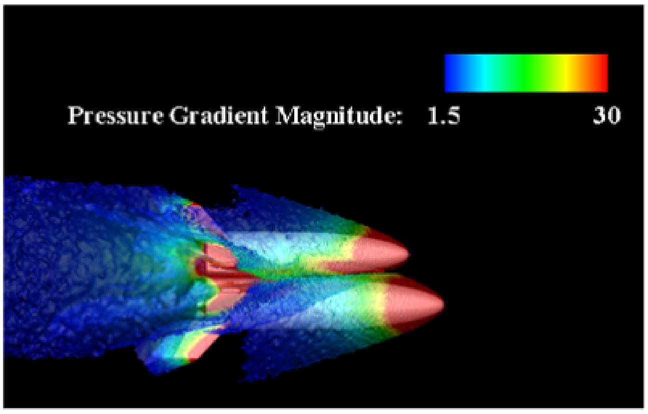

(a)

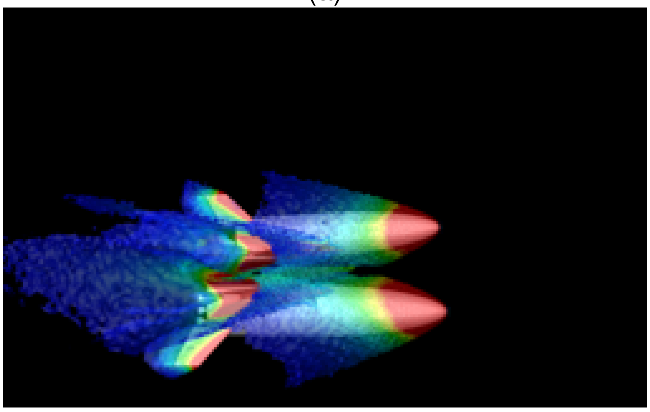

(b)

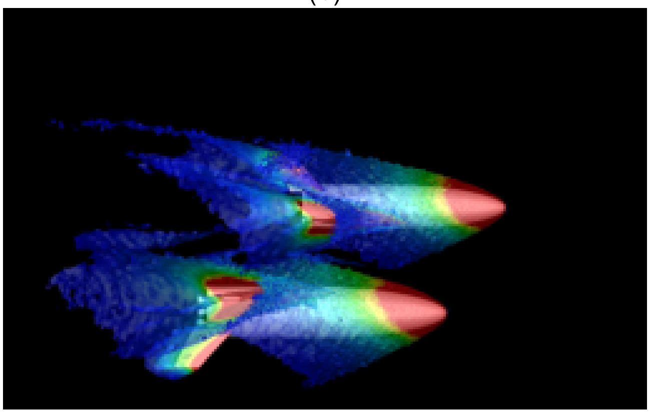

(c)

Figure 7 – Flowfield of obtained solutions.(a)$t = 0.0$, (b)$t = 1.0$, and (c)$t = 2.0$.

References

[1] Kalyanmoy Deb. An efficient constraint handling method for genetic algorithms. *Computer methods in applied mechanics and engineering*, 186(2-4):311–338, 2000.

[2] Takahiro Fujikawa, Koichi Yonemoto, Hiroshi Yamasaki, Masatomo Ichige, Yusuke Ura, Guna S Gossamsetti, Takumi Ohki, Yuki Kubono, Kento Shirakata, Hirotoshi Tsukamoto, et al. Research and development of winged reusable rocket: current status of experimental vehicles and future plans. In *Proceedings on Asia-Pacific International Symposium on Aerospace Technology. JSASS, Soul, Republic of Korea*, 2017.

[3] Yasushi Ito, Alan M Shih, and Bharat K Soni. Unstructured mesh generation using megg3d-mixed-element grid generator in three dimensions. In *Proc. the International Conf. on Numerical Geometry, Grid Generation and Scientific Computing (NUMGRID2008)*, pages 5–11. Citeseer, 2008.

[4] Hiroya Iwafuji, Masahiro Kanazaki, and Takahiro Fujikawa. Plume effect of flowfield around winged two-stage-to-orbit and its flight characteristics. In *AIAA Scitech 2019 Forum*, page 0017, 2019.

[5] Donald R Jones, Matthias Schonlau, and William J Welch. Efficient global optimization of expensive black-box functions. *Journal of Global optimization*, 13(4):455–492, 1998.

[6] Masahiro Kanazaki, Takashi Matsuno, Kengo Maeda, and Hiromitsu Kawazoe. Efficient global optimization applied to wind tunnel evaluation-based optimization for improvement of flow control by plasma actuators. *Engineering Optimization*, 47(9):1226–1242, 2015.

[7] Masahiro Kanazaki, Yuzuru Yokokawa, Mitsuhiro Murayama, Takeshi Ito, Shinkyu Jeong, and Kazuomi Yamamoto. Nacelle chine installation based on wind-tunnel test using efficient global optimization. *Transactions of the Japan Society for Aeronautical and Space Sciences*, 51(173):146–150, 2008.

[8] David Lovely and Robert Haimes. Shock detection from computational fluid dynamics results. In *14th computational fluid dynamics conference*, page 3285, 1999.

[9] F Menter, JC Ferreira, T Esch, and B Konno. The sst turbulence model with improved wall treatment for heat transfer predictions in gas turbines. gas turnine congress (international) proceedings. tokyo. paper no. *Tokyo. Paper*, (IGTC2003):059, 2003.

[10] Shigeru Obayashi and Yasuhiro Wada. Practical formulation of a positively conservative scheme. *AIAA journal*, 32(5):1093–1095, 1994.

[11] Seokkwan Yoon and Antony Jameson. Lower-upper symmetric-gauss-seidel method for the euler and navier-stokes equations. *AIAA journal*, 26(9):1025–1026, 1988.